*Materials and Structures*, 1993, **26**, 532–548

# Cover cracking as a function of rebar corrosion: Part 2—Numerical model

F. J. MOLINA

*Universidad de Oviedo, Departmento de Construcción, Campus de Viesques, 33204 Gijon, Spain*

C. ALONSO, C. ANDRADE

*Instituto de Ciencias de la Construcción Eduardo Torroja, Serrano Galvache s/n, 28033 Madrid, Spain*

*A numerical model based on standard finite-element techniques is proposed for the simulation of cracking in concrete specimens when subjected to corrosion of their reinforcement. A smeared-crack approach is used to model the behaviour of the concrete finite elements, while the corrosion, which is understood as the applied load on the structure, is modelled by a combination of initial strains and change of elastic properties, which are respectively equivalent to the expansion and softening of the steel elements at the rebar surface when they rust. The model is applied to four examples, which were simultaneously tested experimentally and reported in Part 1 of this paper, and the influence of the main parameters of the model in the response is studied separately. In particular, the effect on the crack-width rate of the specific volume of the rust being formed is quantitatively assessed.*

## 1. INTRODUCTION

The degradation of a concrete structure by the corrosion of its reinforcement is clearly a very complex phenomenon which involves multiple causes and effects. From the purely mechanical point of view, it consists of a loss of the rebar cross-section which is transformed into rust. These products of corrosion, depending on several environmental factors, can have different properties, but normally their specific volume is greater than that of the virgin steel; the result is a dilatation of the bar (steel + rust) and consequently the cracking of the surrounding concrete.

To study this phenomenon, some experimental studies have been carried out which, in general, show some interesting features, but suffer two important limitations:

(i) the difficulty of isolating factors, due to the complexity of the phenomenon, and

(ii) the cost and duration of the tests which can take years or at least months, in the case of artificially accelerated corrosion [1].

Obviously, the interest in the development of a numerical model for the study of this problem lies in the possibility of overcoming these drawbacks, after the necessary agreement between experiments and computations is achieved.

Finite-element (FE) modelling of cracking in concrete is currently still under development, but some of the available models are probably accurate enough for the object of our study and have, in fact, been applied to it. For example, Sygula and Ryz [2] and McLeish [3] use FE modelling for the concrete part of the specimen, while the corrosion is modelled by a uniform pressure or dilatation. However, both models could be considered as incomplete because they do not include the rebar as a part of the model and, moreover, before the problem is solved experimentally or by another model, the applied load in each case (pressure or dilatation) cannot be easily related to the time the structure has been exposed to the corrosive conditions.

In our approach, the applied load, say $x$ (independent variable), will be the radial loss, or attack penetration, in the rebar. This penetration will be assumed uniform along the perimeter of the bar. The results of the analysis will be the evolution of the induced cracking in the concrete as a function of that increasing parameter.

To apply the model to a real situation, the speed of corrosion must be known as a function of both the environmental conditions and the type of structure, in order to substitute $x$ by time and then obtain useful information concerning the service life of that structure. However, at this stage, at least two factors of possible significance are not yet covered by the model. These are, on the one hand, the dependence of the said speed of corrosion on the self-induced cracking and, on the other hand, the possible partial expansion effectiveness of the formed rust due to its diffusion through the concrete.

## 2. NUMERICAL MODEL

The proposed model tries to cover the mechanical aspects of the phenomenon under study by the use of a combination of several types of load and material behaviour which are currently available in FE techniques. In fact, this model was previously presented by us [4], but without any experimental data with which to compare.

0025-5432/93 

### 2.1 Simulation of corrosion

Because corrosion is not a standard type of load in the FE codes, its implementaton is made in a special way. The corrosion of a steel element is modelled by the superposition of two effects: a decrease in its stiffness, and an increase in its specific volume.

The first effect is achieved by a linear variation of the properties of the material from those of the steel to those of the rust. The latter properties, considering the present lack of information, are assumed nearly equal to those of the liquid water (which is one of the main components of the rust under these conditions), i.e.

$$\nu_r = 0.5 \tag{1}$$

for the Poisson's ratio and

$$K_r = 2.0\,\text{GPa} \tag{2}$$

for the bulk modulus. It is not possible to use Equation 1 directly within the FE displacement method, but it can be replaced by a value slightly lower than 0.5 [5] and then used to compute a Young's modulus

$$E_r = 3(1 - 2\nu_r)K_r \tag{3}$$

which is small, but not zero. Obviously, these values from Equations 1–3 of the properties of the rust should be replaced by others which are more realistic if a way can be found to obtain them.

Both virgin steel and rust are considered within the model as only one material with properties varying linearly.

The second effect (increase in volume) is achieved by the imposition of an initial strain on the element being corroded. Calling

$$v_{r/s} = v_r/v_s \tag{4}$$

the ratio between the specific volumes of rust and steel, the isotropic initial strain to impose on the diagonal components of the strain tensor is

$$\varepsilon_x^0 = \varepsilon_y^0 = \varepsilon_z^0 = \frac{(v_{r/s} - 1)}{3} \tag{5}$$

when infinitesimal strain theory is applicable. Unfortunately, the said theory is not strictly applicable because the value of $v_{r/s}$ is about 2, as has been observed in the examples of this work. Nevertheless, the infinitesimal strain model is recommended by us due to its simplicity and because, surprisingly, even in the case of an important change in volume, considering certain present conditions of symmetry, the initial strains (Equation 5) can still give a good approximation for this problem, as justified in Appendix A.

As we proposed [4], both corrosion effects can be obtained simultaneously by a single thermal load if the FE code allows temperature-dependent properties as well as thermal expansion. In that case it must be verified, where $\alpha$ is the coefficient of thermal expansion and $\Delta T$ the increment of temperature, that

$$\alpha\Delta T = \frac{(v_{r/s} - 1)}{3} \tag{6}$$

However, we now propose to introduce a time lapse between both effects, so that an element is not expanded before being fully softened, since in this way some unrealistic tensions inside the rebar are eliminated.

### 2.2 Simulation of cracking

Within both basic categories (discrete and smeared) of crack models for concrete developed in FE analysis, the smeared-fixed-crack model with linear softening proposed by Rots *et al.* [6] has been chosen by us because of its relatively easy implementation and its clear presentation. The fundamentals of this model are included in Appendix B for completeness.

However, hopefully, the type of crack model implemented for this problem should not be the primary determinant with respect to the results, since mode I fracture is the type of crack mainly observed in the examples and both discrete and smeared models usually give coincident results for such a mode of fracture [7].

## 3. EXAMPLES

### 3.1 Materials and experimental results

The first part of this work [1] contains the results of four corrosion tests which were carried out to obtain useful experimental data in the validation of the numerical model proposed here. That information is summarized as follows.

The specimens were made of a 30 MPa resistant concrete with a measured splitting tensile strength of 3.55 MPa. In order to induce uniform accelerated corrosion in the rebar, a fixed electric current was applied between the bar and a counterelectrode. Assuming that the entire current $I$ was consumed in the oxidation, the attack-penetration increment was estimated as

$$\Delta x = 0.032 I\,\Delta t \quad (\mu\text{m}) \tag{7}$$

where $I$ was 100 $\mu$A cm$^{-2}$ (or 10 $\mu$A cm$^{-2}$ for specimen IV) and $\Delta t$ was the time increment in days. The initial value of radius loss was also estimated by measurement of the polarization resistance [1].

The histories of the strains, measured by the strain gauges at the surface, are plotted in Fig. 1, where the abscissa represents the time, as well as the attack penetration $x$ estimated by Equation 7, and the ordinate represents the strain, as well as the crack width estimated by

$$w = L\varepsilon \tag{8}$$

$\varepsilon$ being the strain at the gauge and $L$ its length (30 mm in this case). For compactness, Fig. 1 also includes the analytical results obtained with the numerical model (dashed line), but the comparison is postponed until the discussion.

### 3.2 Applied model and analytical results

Within the numerical model, the values adopted for its parameters were the following:

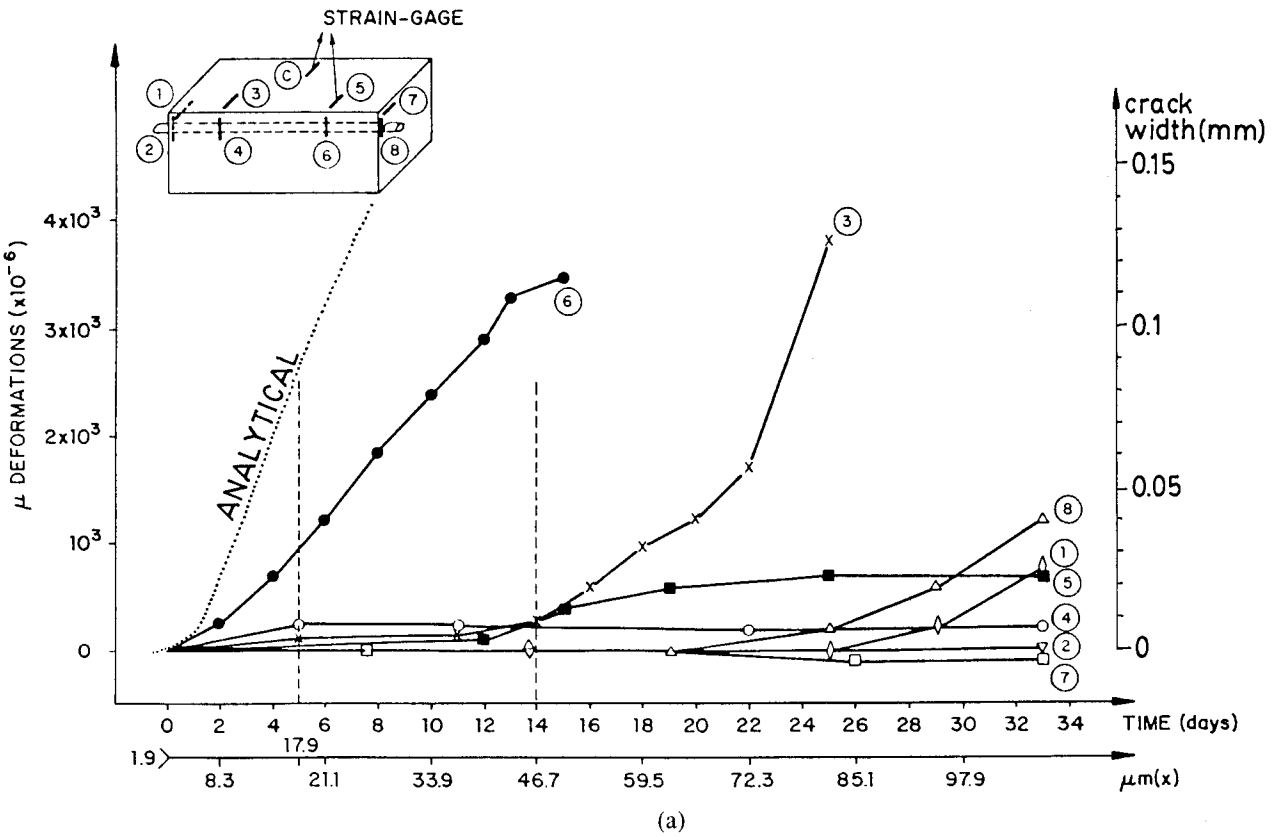


(a)

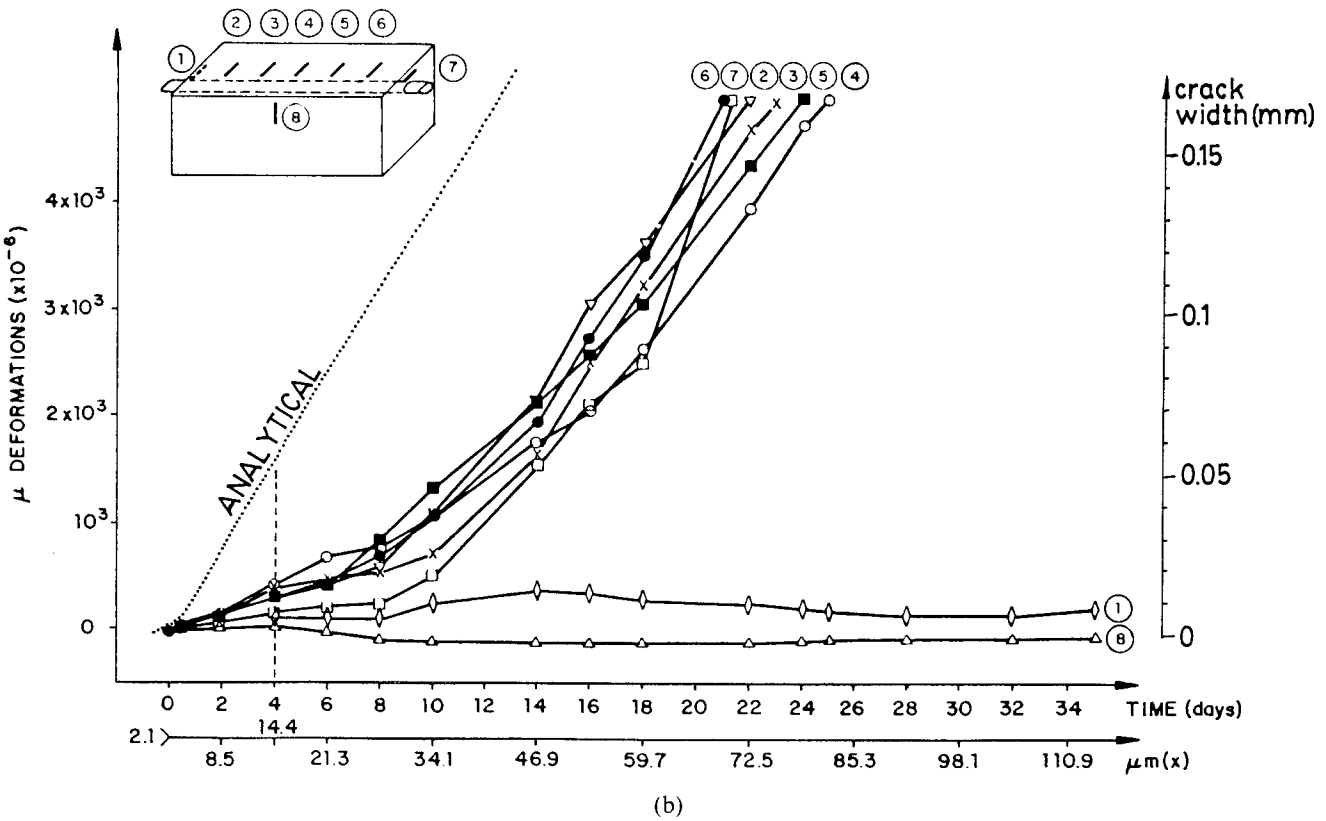


(b)

Fig. 1 Experimental results from Part 1 [1]: (a) specimen I, (b) specimen II. (*continued*)

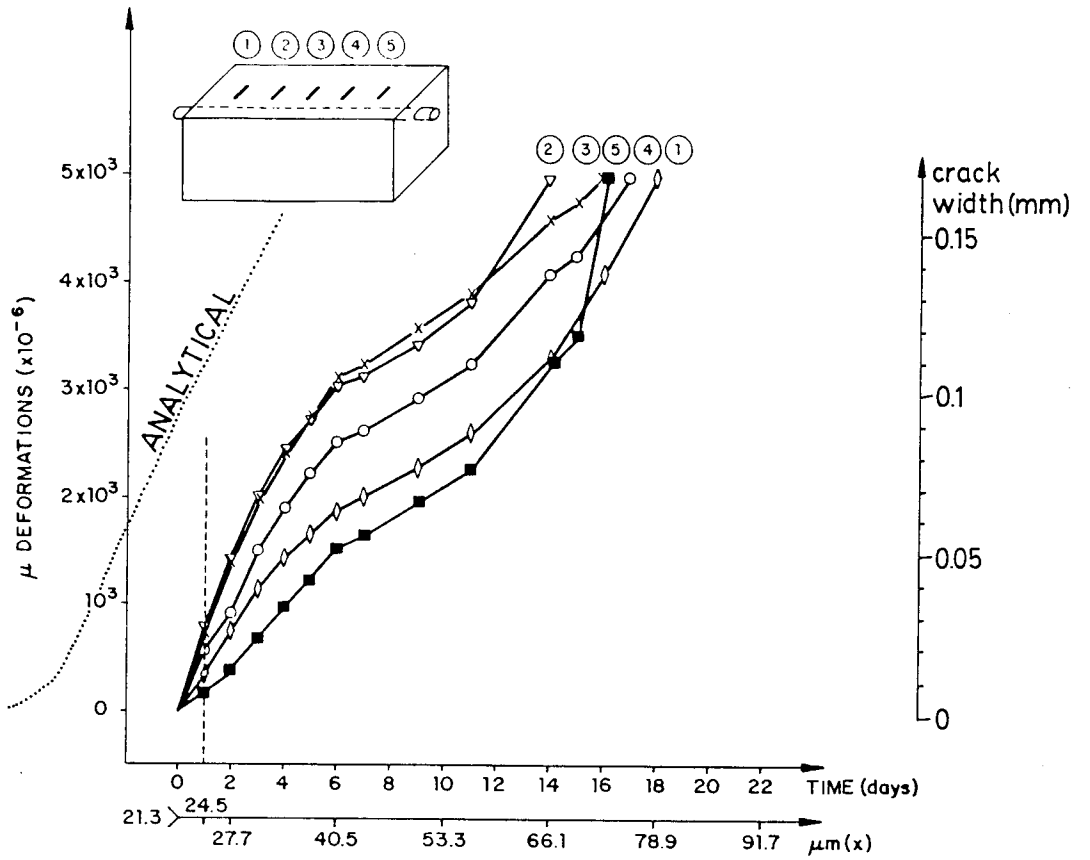


(c)

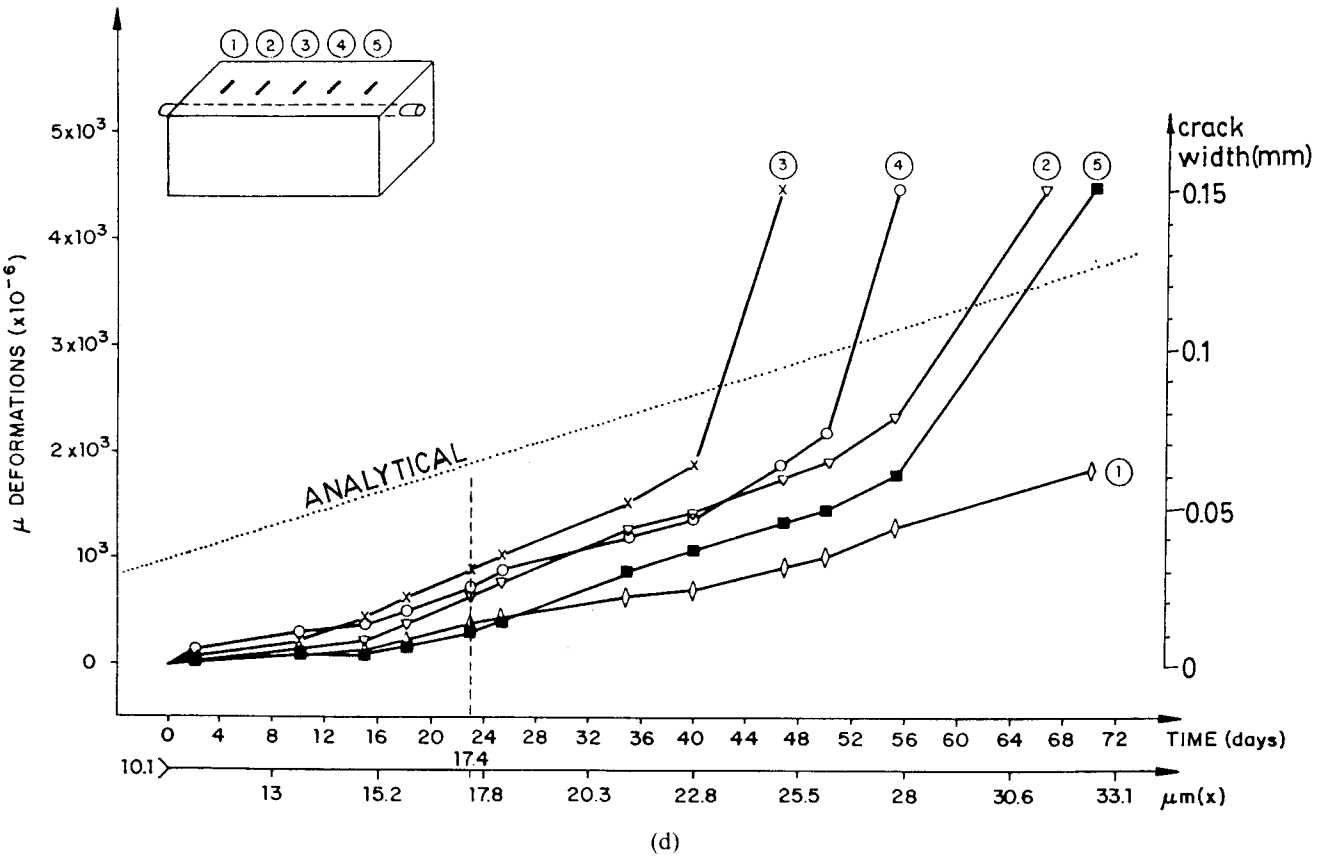


(d)

Fig. 1 *continued* (c) specimen III, (d) specimen IV.

(i) For the virgin steel (elastic)

$$E_s = 210\ \text{GPa} \qquad \nu_s = 0.3 \tag{9}$$

(ii) For the rust (elastic)

$$K_r = 2.0\ \text{GPa} \qquad \nu_r = 0.499 \qquad \upsilon_{r/s} = 2.0 \tag{10}$$

(iii) For the concrete (smeared-crack)

$$E_c = 36\ \text{GPa} \qquad \nu_c = 0.2$$
$$f_{ct} = 3.55\ \text{MPa} \qquad G_f = 200\ \text{J m}^{-2} \qquad \beta = 0.2 \tag{11}$$

where the properties of the rust were estimated as explained above and the properties of the concrete were either measured (in the case of the tensile strength $f_{ct}$) or taken from the literature. It must be observed that the measurement of properties like the fracture energy $G_f$ or the shear retention factor $\beta$ would have required very specialized equipment [8] which was not available to us.

A mesh of eight-node plane-strain elements was created to model the cross-section of each of the specimens (Fig. 2) using three layers of very thin elements (20 μm, not visible in the figure) of rustable steel at the surface of the rebar in order to properly graduate the simulation of uniform corrosion, layer by layer. In the case of the mesh for the first specimen (Fig. 2a), the ideal symmetry was altered by introducing on the left a cover 1 mm greater than the nominal, just to force the appearance of the main crack in the ascending direction (12 h in a clock reference) as was observed in the test.

The corrosion was simulated by the application of three cumulative load combinations, each representing an advance of 20 μm in the attack penetration. The integration was performed by the incremental version of the modified Newton–Raphson algorithm [5] with simultaneous checking of force and displacement errors and by using a secant-stiffness approach.

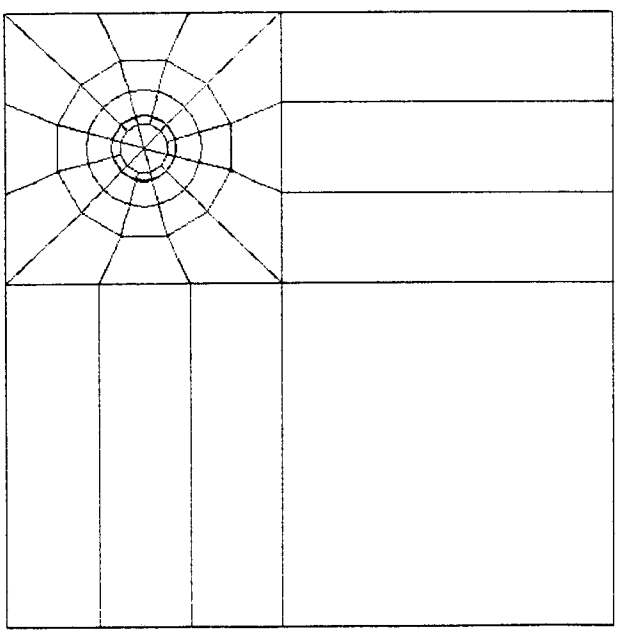

(a)

Fig. 2 Finite-element meshes: (a) specimen I. (*continued*)

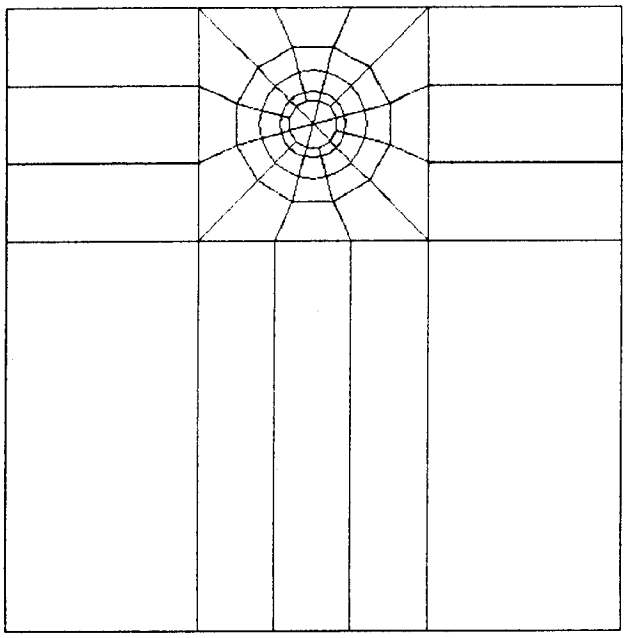

(b)

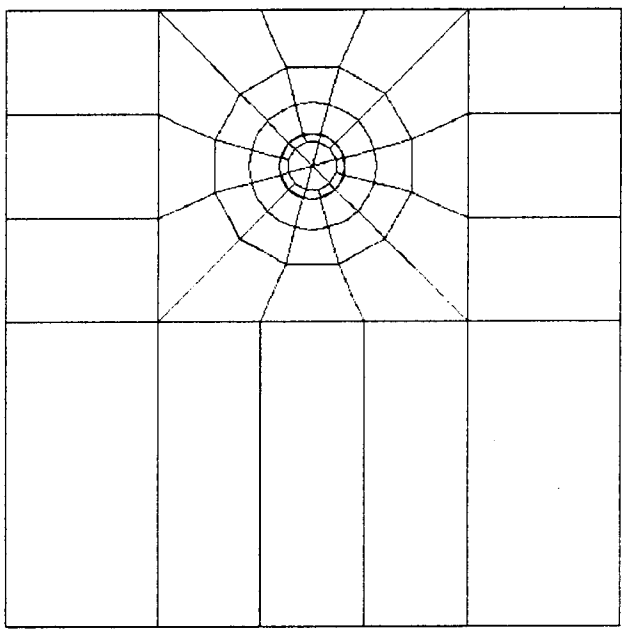

(c)

Fig. 2 (*continued*) (b) specimens II and IV, (c) specimen III.

Figs 3a, 4a and 5a show the final deformed meshes with the resultant cracking for $x = 60$ μm. At each integration point, a segment represents the direction of cracking (if any), its width being proportional to the crack width using the same magnification as in the displacements (30 times). Consequently, even though the cracking is present in all radial directions, it is only noted in those directions where significant crack widths are developed, that is to say, using a clock reference:

(i) Specimen I: main crack at 12 h, secondary crack at 4.30 h.

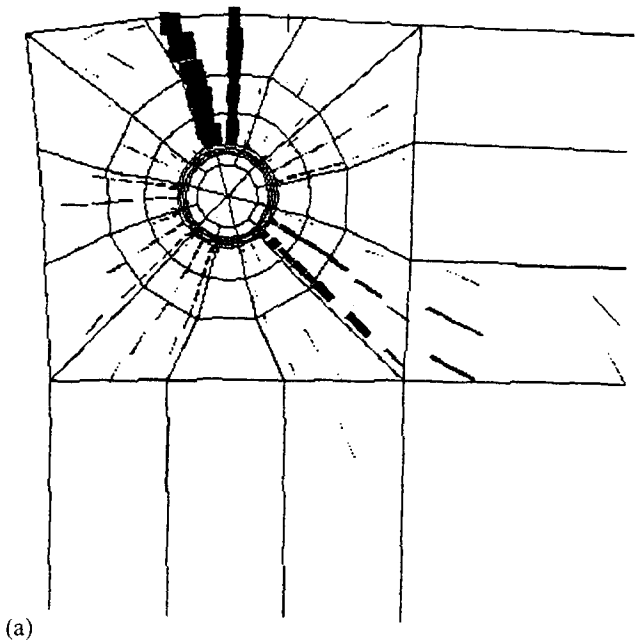

(a)

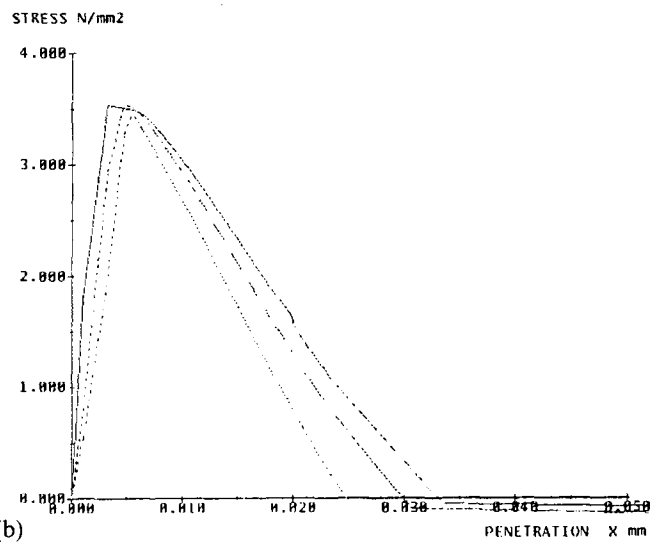


(b)

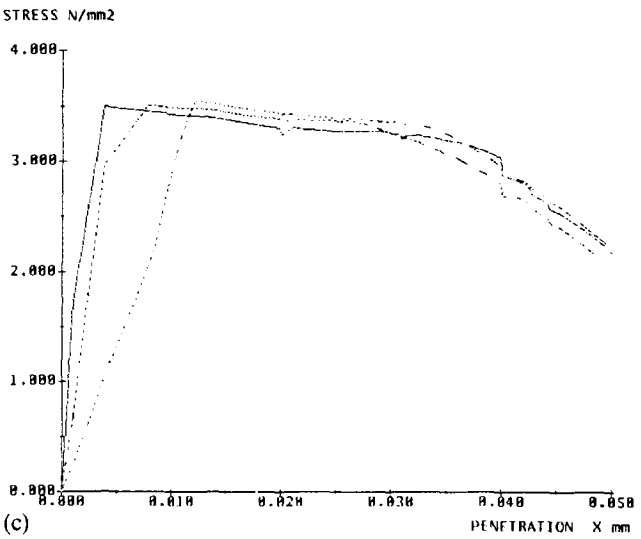


(c)

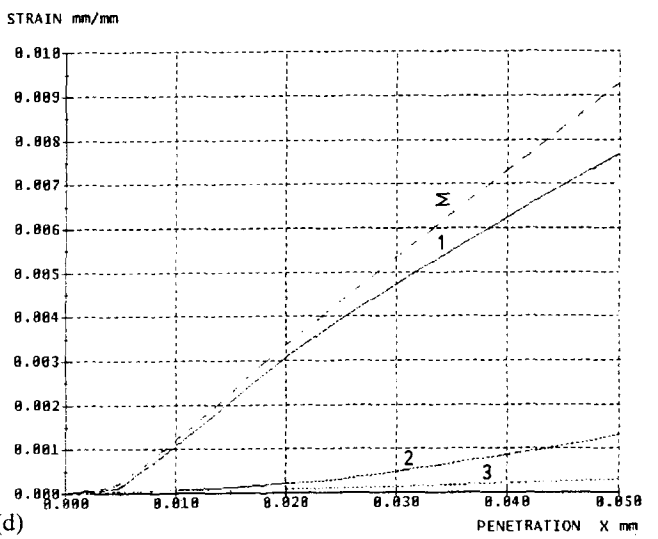


(d)

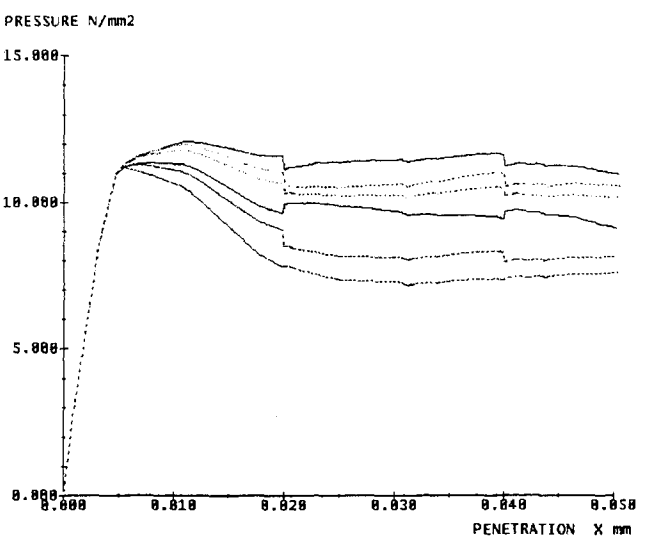


(e)

Fig. 3 Results for specimen I: (a) deformed mesh with cracks, (b) normal stress at main crack, (c) normal stress at secondary crack, (d) average normal strain, (e) pressure at rebar.

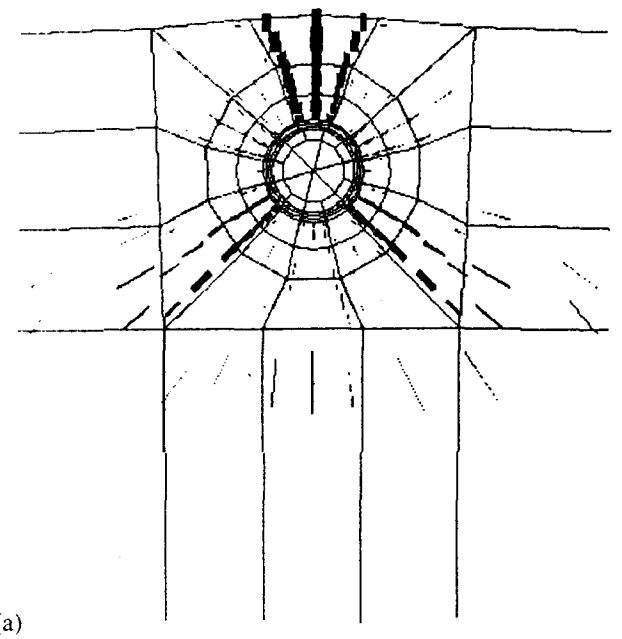

(a)

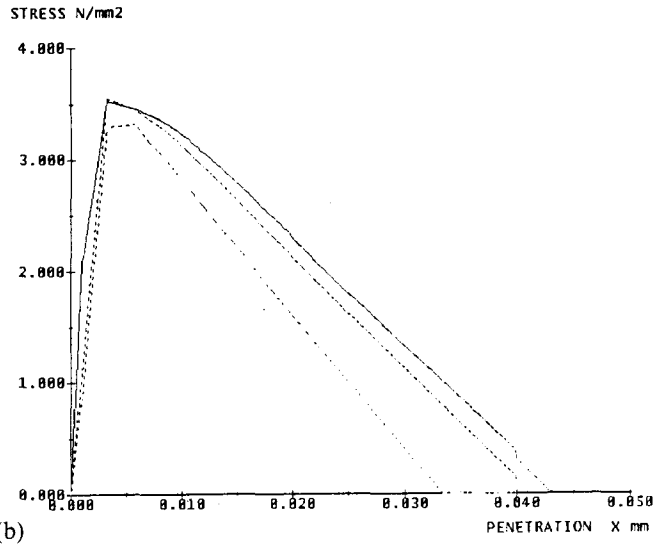


(b)

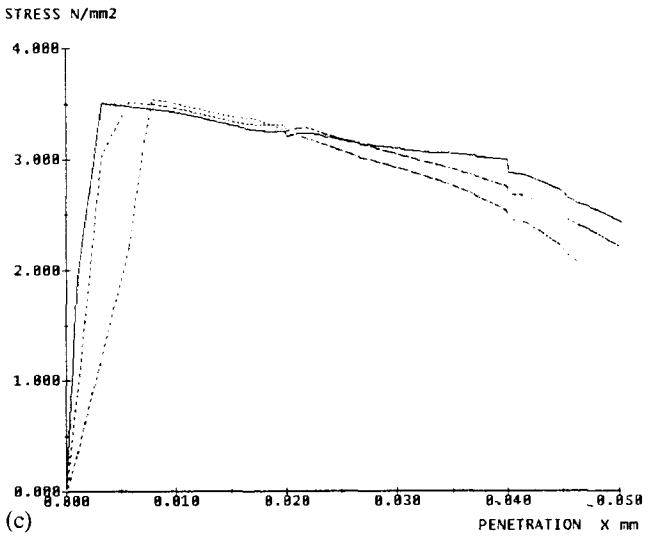


(c)

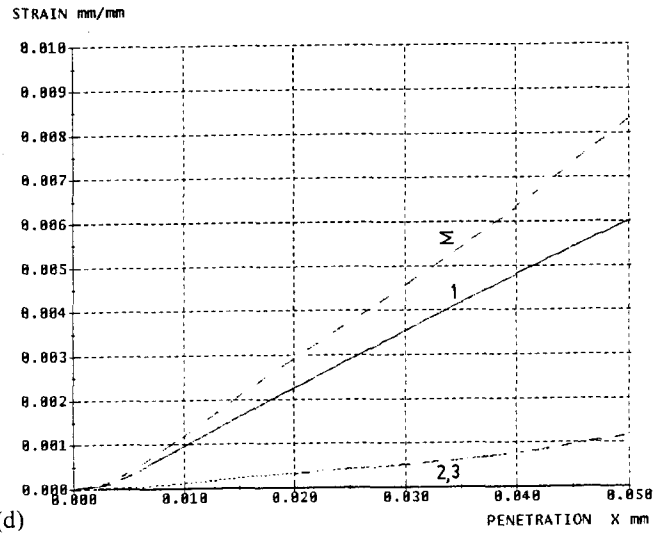


(d)

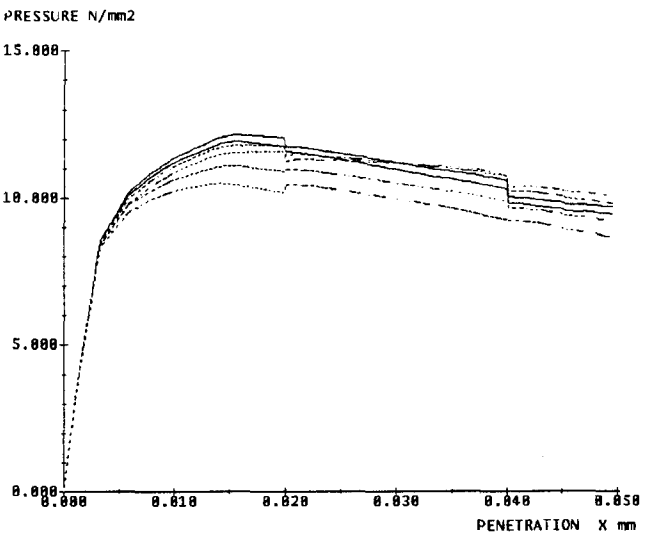


(e)

Fig. 4 Results for specimens II and IV: (a) deformed mesh with cracks, (b) normal stress at main crack, (c) normal stress at secondary crack, (d) average normal strain, (e) pressure at rebar.

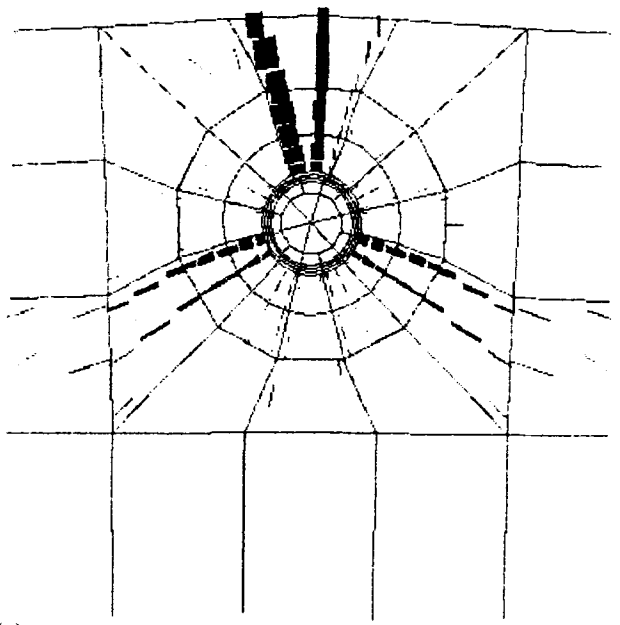

(a)

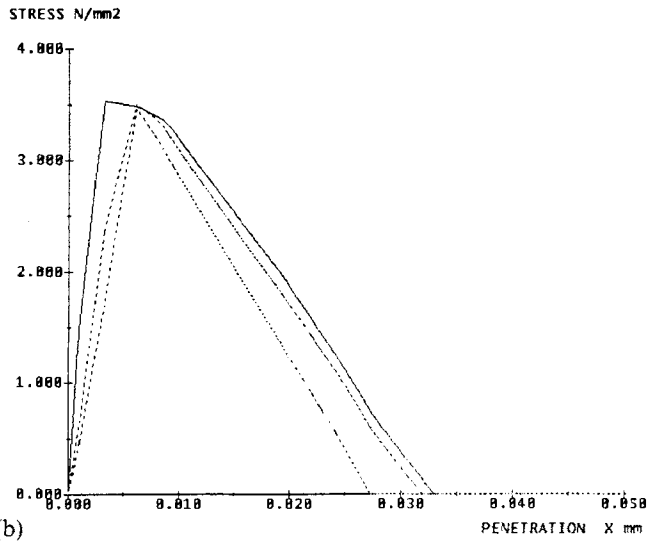


(b)

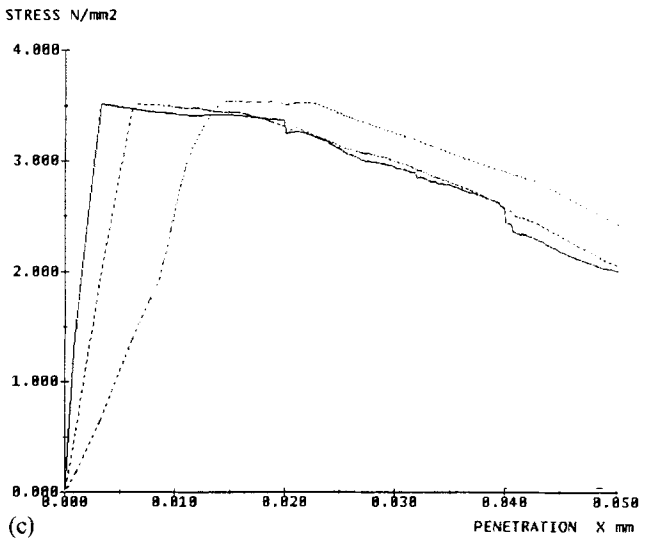


(c)

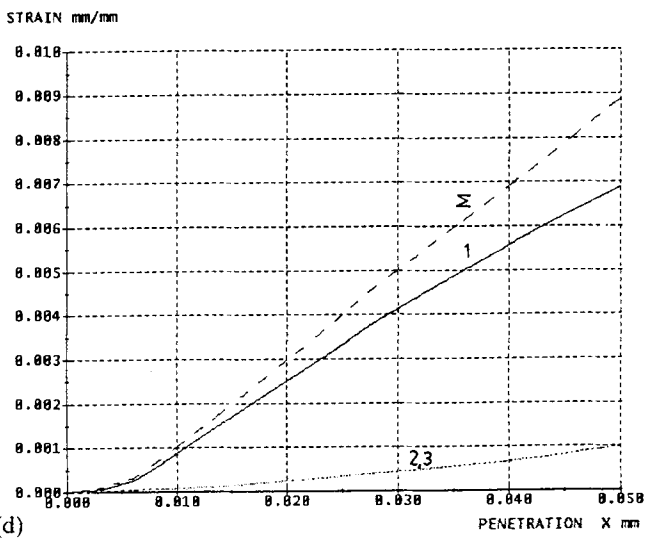


(d)

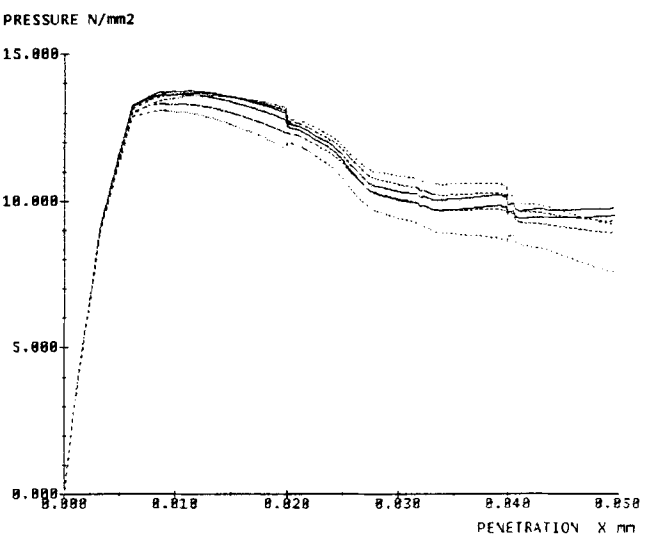


(e)

Fig. 5 Results for specimen III: (a) deformed mesh with cracks, (b) normal stress at main crack, (c) normal stress at secondary crack, (d) average normal strain, (e) pressure at rebar.

(ii) Specimens II, III and IV: main crack at 12 h, secondary cracks at 4.30 and 7.30 h.

It is observed that the crack widths are not fully localized, which is a common occurrence in the smeared-crack model [6] and, probably, is also an analytical interpretation of the lack of uniformity in the cracking pattern along the depth of the test specimens. The asymmetric crack distribution obtained for specimen III (Fig. 5a) is possibly due to the intrinsic instabilty of the softening model.

Figs 3b, 4b and 5b show the evolution of the main-crack normal stress registered in the three elements of the concrete cover. According to these results, the crack is initiated (microcracking at the deepest element (solid curve in the graphs) and then is propagated to the external ones which reach the tensile limit ($f_{ct} = 3.55$ MPa) a bit later. However, the crack first becomes totally opened, consuming the whole fracture energy (macrocracking), at the most external element. For all the specimens, the main crack is initiated and propagated between penetrations of about 2 and 8 μm, the normal stress becoming zero for penetrations which range from 20 to 50 μm.

In the same way, Figs 3c, 4c and 5c show the evolution of the secondary-crack normal stress registered in the first three element layers that surround the rebar. It is observed that the secondary crack is initiated (microcracking) at the same time as the main crack ($x \simeq 2$ μm) at the steel–concrete interface, but its propagation to the surface is a bit slower and its full opening can take much longer. Physically, for these examples, the said full opening of the secondary crack would mean the detachment of a piece of cover, since no stirrups were present.

In order to obtain results to compare with those of the tests, the measurement at the gauges was simulated by computation of the relative displacement between two nodes (one at each side of the main crack in the surface) divided by 30 mm. The evolution of this average strain is represented as a solid line labelled 1 in Figs 3d, 4d and 5d. As in the experimental case, the conversion from strain to crack width is made by use of Equation 8. These same three curves have been copied in Fig. 1 as dashed lines in order to establish a comparison between experimental and analytical results in the discussion.

The same Figs 3d, 4d and 5d also include the strain registered at other simulated gauges (not existing in the test), labelled 2 and 3, and the summation labelled Σ, of the three strains. The exact situation of all the gauges is shown in Fig. 6. It can be observed that, although the strain at the main crack presents important variations from specimen to specimen, the summation of strains at the three principle cracks is very similar among all the specimens. In quantitative terms, considering that the curves are more or less straight lines which intersect the origin, Table 1 displays the secant rate of strain (obtained by dividing the final value in the graph by a penetration of $x = 0.050$ mm).

The same table includes the corresponding crack-width

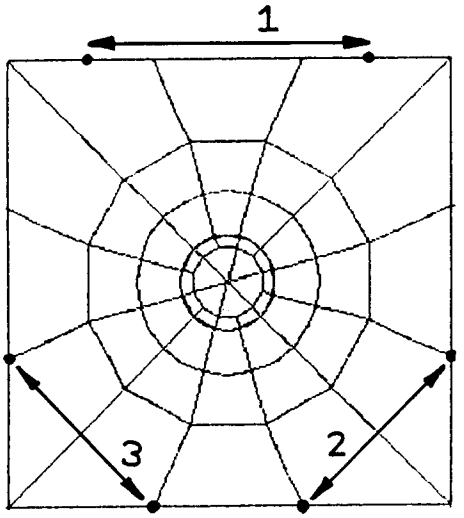


Fig. 6 Location of simulated strain gauges.

rates $w/x$, obtained by multiplying the strain rates by the assumed common gauge length of 30 mm. The sum of width rates is also necessarily observed as rather stable among the specimens. In fact, if the fracture energy is completely released in all the cracks and an ideal stress-free state is assumed, the problem becomes a purely geometric one and the sum of width rates in all the cracks is almost exactly

$$\sum \frac{w_i}{x} = 2\pi(v_{r/s} - 1) \tag{12}$$

as shown in Appendix C, which, by Equation 10, for these examples becomes

$$\sum \frac{w_i}{x} = 6.3 \tag{13}$$

This value is greater than those recorded in Table 1, probably because the latter include only three cracks instead of all, and the fracture energy has not yet been completely consumed in the model. Anyway, what is significant is that Equation 12 could be used as a practical conservative bound for the asymptotic crack growth with respect to the radius loss, at least within the assumptions of the numerical model.

Finally, Figs 3e, 4e and 5e contain the evolution of

Table 1 Analytical crack-width rates for $x = 0.05$ mm

| | Specimen I | Specimens II and IV | Specimen III |
|---|---|---|---|
| $\varepsilon_1/x$ (mm$^{-1}$) | 0.154 | 0.120 | 0.137 |
| $w_1/x$ | 4.6 | 3.6 | 4.1 |
| $\sum_1^3 (\varepsilon_i/x)$ (mm$^{-1}$) | 0.186 | 0.168 | 0.178 |
| $\sum_1^3 (w_i/x)$ | 5.6 | 5.0 | 5.3 |

pressure, computed by

$$p = -\frac{\sigma_x + \sigma_y}{2} \tag{14}$$

where $\sigma_x$ and $\sigma_y$ are the in-plane normal stress components registered at the six elements in the centre of the rebar. This result is included here for completeness, because in other tests the corrosion is simulated by an applied pressure on a fluid which fills the bar [9]. It is observed that the pressure presents a maximum (between 11 and 14 MPa, depending on the specimen), which can constitute a serious impediment for a pressure-control test since, at that point, the test would finish abruptly.

## 4. DISCUSSION

### 4.1 Validity of the numerical model

The proposed numerical model is mainly based on established numerical approximation techniques. Hence, its consistency has been only partially tested (Appendix D). However, the generality of the said consistency follows from the proper use of such techniques and the checking of the assumptions introduced.

On the other hand, prior to the comparison of the analytical and experimental results (Fig. 1), it must be kept in mind that some of the parameters which can strongly affect the results were arbitrarily chosen in the numerical model. This is especially the case for the specific volume of the rust which is a determinant variable for the strain rate, as shown in Appendix E. Another observation to be made is that the relation between days and penetration (Equation 7) as well as the initial value of the penetration were obtained under simple assumptions which could be strengthened in future work. There also exists an unknown magnitude in these figures which is the offset in the initial value of the experimental strain.

For the first specimen (Fig. 1a) the analytical strain rate is perhaps too high, but the existing scatter in the experimental values for this specimen does not allow a definitive conclusion. However, for the second specimen (Fig. 1b), the experimental dispersion is low and the analytical strain rate is of the order of the experimental one. Nonetheless, the experimental curves present a growing slope which could not be easily reproduced by the present numerical model. We believe that the initial value of the experimental strain rate is comparatively small due to a diffusion of the earlier formed rust into the surrounding porous concrete. When the latter is saturated, the expansion effect is consequently larger. In fact, with other tests of controlled expansion not involving corrosion (not yet reported), we have obtained the uniform type of response predicted by the numerical model.

For specimen III (Fig. 1c), the dispersion is low and the experimental strain rate is relatively well reproduced by the model. The experimental decrease of the rate after $x = 40$ μm is not observed in the analytical results and could be due to a migration of the rust through the opened crack [1]. Finally, for specimen IV (Fig. 1b), the slope of the experimental data is only well reproduced initially, particularly before $x \simeq 23$ μm, since afterwards the experimental slopes grow considerably.

### 4.2 Interpretation of results

Although the proposed model needs more comparison with experimental data for its validation and for the adjustment of its parameters, the results of the examples that have been treated could supply interesting information about the phenomenon (see with respect to this the study of parameter sensitivity contained in Appendix E).

For example, if the growth of the main crack is considered as the principal determinant for service life of the reinforced concrete element, the most important datum to investigate is probably the specific volume of the rust being formed, once the speed of corrosion has been estimated. It has been shown by the results of Appendix E that, within the numerical model, only a change of that specific volume produces a strong effect on the crack-width rate.

In relation to the effect of the mechanical properties of the concrete it can be said that, for a constant geometry, they may only affect the evolution of cracking during the initial phases of crack creation at the interface with the rebar and its propagation to the surface, but not during the subsequent crack growth. With the aid of other studies, we have confirmed that a ductility number, such as the one indirectly proposed by Hillerborg *et al.* [10], and whose definition could be

$$\delta = \frac{G_f E_c}{L_s f_{ct}^2} \tag{15}$$

$L_s$ being the size of the specimen section, is the one that controls the initial delay in the crack growth which was observed when the Young's modulus was diminished. However, with respect to the maximum pressure developed in the rebar, the tensile strength is determinant if the geometry is not altered.

## 5. CONCLUSIONS

From the comparison of the experimental and analytical results, a definitive validation of the proposed numerical model is not yet possible, but it can be said that it is capable of reproducing some of the main characteristics of the experimental behaviour with success. Further comparison with new experimental data and improvement of the model are needed as well as the development of testing procedures for adjustment of the most significant parameters, such as the specific volume of the rust.

For the type of problem that has been studied, a determinant influence of the said specific volume on the crack growth has been shown by the numerical results of Appendix E and also by the theoretical development made in Appendix C based upon simple geometrical

considerations. As is clear in Equation 12, the asymptotic global crack-width rate with respect to the penetration of corrosion is proportional to the relative increase in volume of the steel when rusted, $2\pi$ being the factor of proportionality. Such an asymptotic global rate could be used as a conservative limit for the width rate of the main crack; it does not depend on other properties of the materials or on the geometry of the specimen (including the depth of the cover), which only affects the way the global width rate is distributed among the cracks. However, the experimental results allow us to see the relevance in the phenomenon of some factors not yet included in either numerical or geometrical models. One of these factors could be the diffusion of the rust within the concrete and through the cracks, which could indeed be affected, for example, by the geometry of the specimen.

These preliminary conclusions must be confirmed once the model has been better elaborated and extensive parametric studies have been carried out, possibly leading to new and interesting conclusions.

## APPENDIX A:. Justification of the applicability of small-strain theory

Using here for convenience cylindrical coordinates, within the theory of infinitesimal strain, the volumetric strain is defined as

$$e = \varepsilon_r + \varepsilon_\theta + \varepsilon_z \tag{A1}$$

while, if large strain is considered, the unit volume change is better approximated by

$$\varepsilon_v = (1 + \varepsilon_r)(1 + \varepsilon_\theta)(1 + \varepsilon_z) - 1 \tag{A2}$$

In order to show how $e$ can give a good estimation of $\varepsilon_v$ for this problem, it will be considered firstly that a plane strain model is applicable to the cross-section of the specimen, as is reasonable in the examples here considered, so that

$$\varepsilon_z = 0 \tag{A3}$$

and secondly that, taking the origin of coordinates in the centre of the rebar, axisymmetric dilatation of the rust is credible, so that

$$\varepsilon_\theta \simeq \frac{u_r}{r} \simeq \frac{\varepsilon_r X}{r} \tag{A4}$$

where $r$ is the radial coordinate, $u_r$ is its associated displacement and the strain of the steel is assumed much smaller than that of the rust. Under these assumptions and limiting the analysis to a maximum penetration of the order of $r/100$, it is clear that

$$\varepsilon_\theta < \frac{\varepsilon_r}{100} \tag{A5}$$

and then

$$e \simeq \varepsilon_v \simeq \varepsilon_r \tag{A6}$$

Thus, the imposition of an initial volumetric strain of value

$$e^0 = (v_{r/s} - 1) \tag{A7}$$

as made in Equation 5, is equivalent to imposing

$$\varepsilon_v^0 = (v_{r/s} - 1) \tag{A8}$$

as was to be shown.

## APPENDIX B: Fundamentals of the adopted smeared-crack model

The adopted smeared-crack model [6] is based on continuum mechanics and in its formulation is very similar to an elastoplastic model. When the cracking criterion (maximum principal stress criterion) is verified, a crack is created in the direction normal to the principal stress and the strain tensor is decomposed into

$$\boldsymbol{\varepsilon} = \boldsymbol{\varepsilon}^e + \boldsymbol{\varepsilon}^{cr} \tag{B1}$$

where the first term on the right is the elastic strain and the second one is the crack strain. While the relationship between the stress and the elastic strain obeys the linear isotropic elastic law, the relationship between the said stress and the crack strain is defined as an orthotropic softening law which depends on the history of the crack and is given in the differential form

$$\mathrm{d}\boldsymbol{s}^{cr} = \boldsymbol{D}^{cr}\,\mathrm{d}\boldsymbol{e}^{cr} \tag{B2}$$

where $\boldsymbol{s}^{cr}$ are the components of the stress in local coordinates of the crack, $\boldsymbol{e}^{cr}$ are the components of the crack strain in the same reference and $\boldsymbol{D}^{cr}$ is a diagonal matrix. The non-zero coefficients of this matrix are obtained from the diagrams of behaviour in normal and tangent directions to the crack reproduced in Fig. B1, where linear softening is adopted.

The area under the line of Fig. B1a is $G_f/h$, where $G_f$ is the fracture energy of the concrete and $h$ is the crack band width for the smeared strain within the FE mesh.

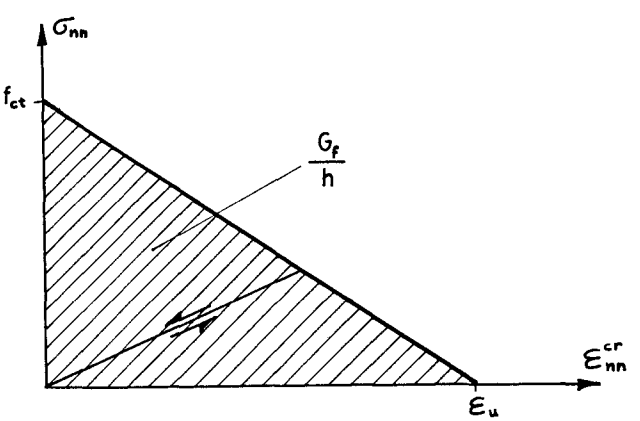


(a)

Fig. B1 Stress–strain behaviour in the crack (after Rots *et al.* [6]): (a) normal traction versus normal strain. (*continued*)

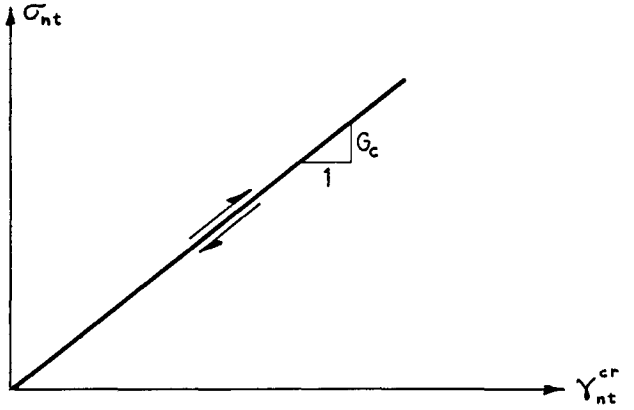


(b)

Fig. B1 (*continued*) (b) shear stress versus shear strain.

Improved recommendations for the selection of $h$ as a function of the type of element used are also given by Rots [11]. The slope of the line in Fig. B1b is

$$G_c = \beta E_c \tag{B3}$$

where $\beta$ is the shear retention factor and $E_c$ is the Young's modulus of the concrete.

## APPENDIX C: Derivation of the formula for an asymptotic crack-width rate

Assuming that a finite number of cracks are completely opened in the concrete that surrounds the rebar and the state is free of stress, the differential increments in the crack widths will be labelled $dw_1, dw_2, dw_3, \ldots$ and the associated uniform penetration of corrosion, $dx$, as shown in Fig. C1. In this state, the net increment of volume of the rusted bar is

$$dV_{net} = (v_{r/s} - 1)2\pi r H\, dx \tag{C1}$$

which corresponds to an increment of its external radius

$$dR = \frac{dV_{net}}{2\pi R H} = (v_{r/s} - 1)\frac{r}{R}dx \tag{C2}$$

and to an increment of its external perimeter

$$2\pi\, dR = 2\pi(v_{r/s} - 1)\frac{r}{R}dx \tag{C3}$$

$r$ being the current radius of the virgin steel and $H$ the depth of the plane model. Now, assuming that the elongation (Equation C3) is absorbed in the concrete by merely incrementing the crack widths, it follows that

$$\sum \frac{dw_i}{dx} = 2\pi(v_{r/s} - 1)\frac{r}{R} \tag{C4}$$

which results in Equation 12 if $r/R$ is approximated by unity and a backward integration is performed to zero.

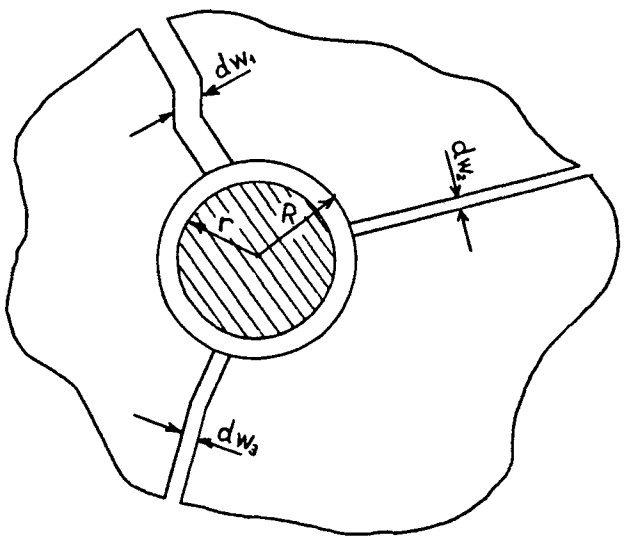


Fig. C1 Geometrical model.

## APPENDIX D: Study of model consistency

In order to test the consistency of the proposed numerical model with respect to some of its parameters which are partially arbitrary, specimen I was re-analysed with different data and the results were compared with those contained in Fig. 3.

First, a refined mesh model with twelve layers of rustable steel elements and five layers of concrete elements in the cover was analysed. Not one of the material properties (Equations 9–11) was altered. The results fitted quite well with those of the original mesh, except perhaps for the final part of the stress at the secondary crack which opened more slowly with this refined mesh. The crack patterns were also comparable.

In the second case, only the Poisson's ratio of the rust was altered from the original data by taking $v_r = 0.4999$, which is nearer to 0.5 than in Equation 10. The results were almost exactly the same as the original ones.

In the third case, the shear retention factor was diminished to $\beta = 0.1$ which produced only minor changes in the results, except for the secondary crack which probably presents a mixed-mode fracture.

The consistency of the numerical model with respect to the size of the load increments and the tolerance to error for the solution was also tested separately for specimen I with success.

## APPENDIX E: Study of parameter sensitivity

This study was limited to specimen I which was re-analysed by changing each of its main parameters separately, but maintaining the original geometry and mesh. The results are collected in Figs E1–4 and must be compared with the original ones in Fig. 3.

The effect of an increase in the ratio between the specific volumes of rust and steel, which was augmented to

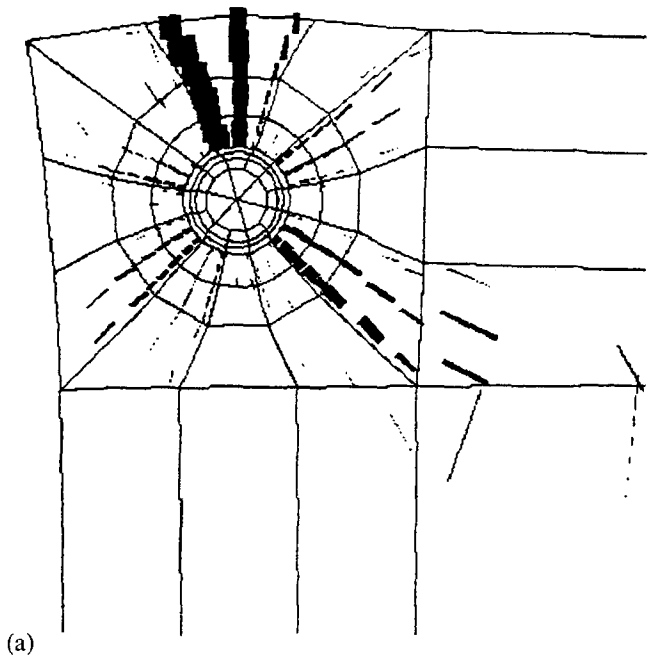

(a)

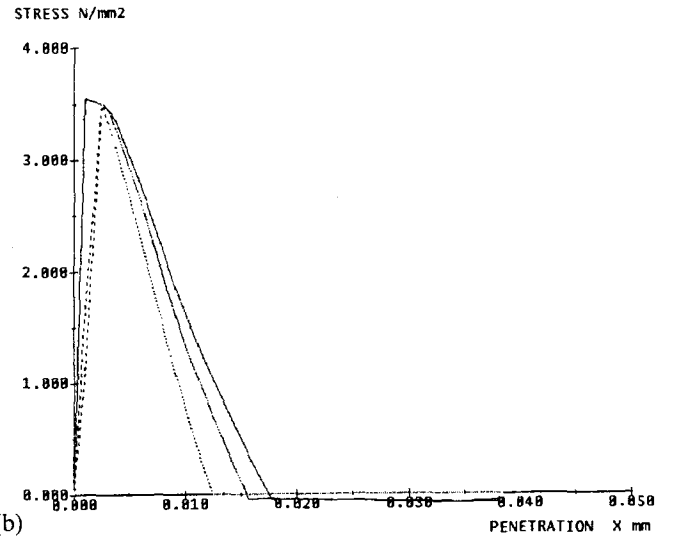


(b)

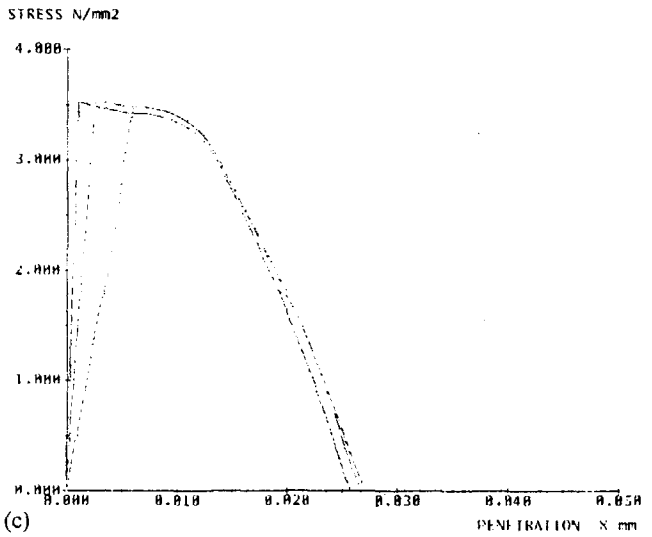


(c)

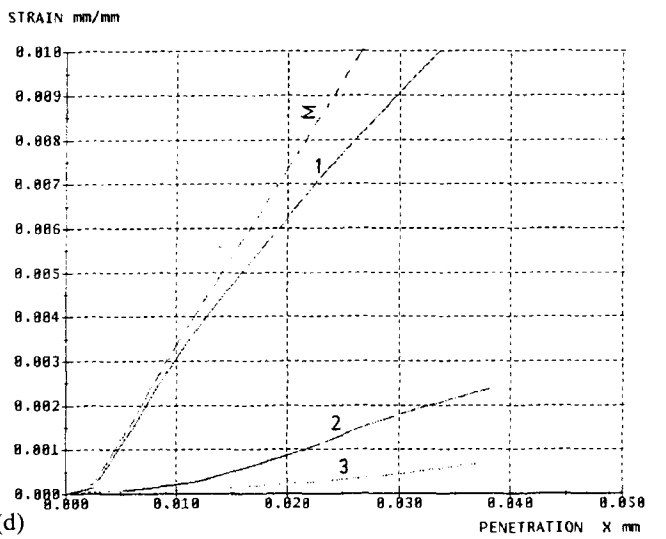


(d)

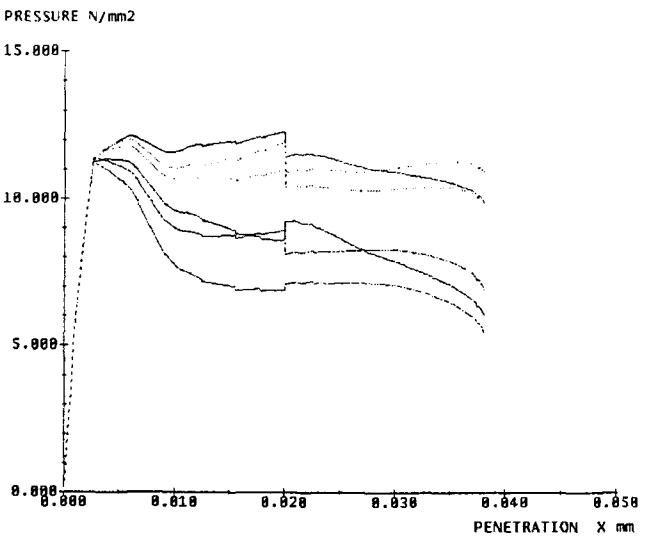


(e)

Fig. E1 Results for specimen I (specific volume of rust augmented): (a) deformed mesh with cracks ($x = 0.04$ mm), (b) normal stress at main crack, (c) normal stress at secondary crack, (d) average normal strain, (e) pressure at rebar.

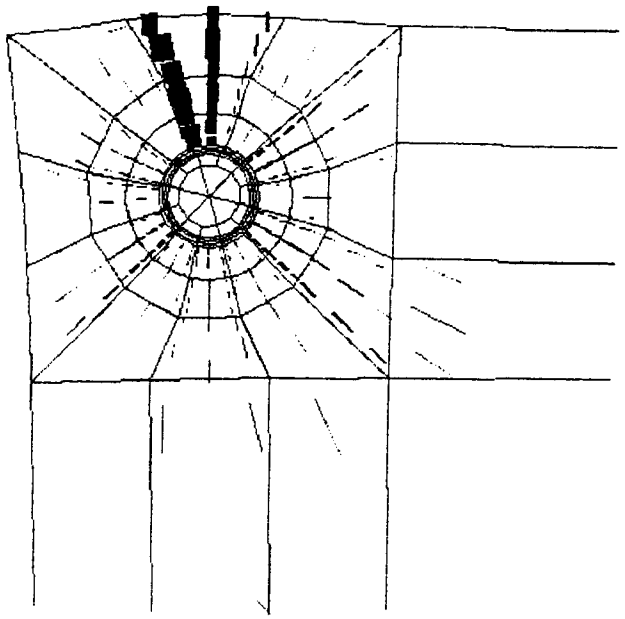

(a)

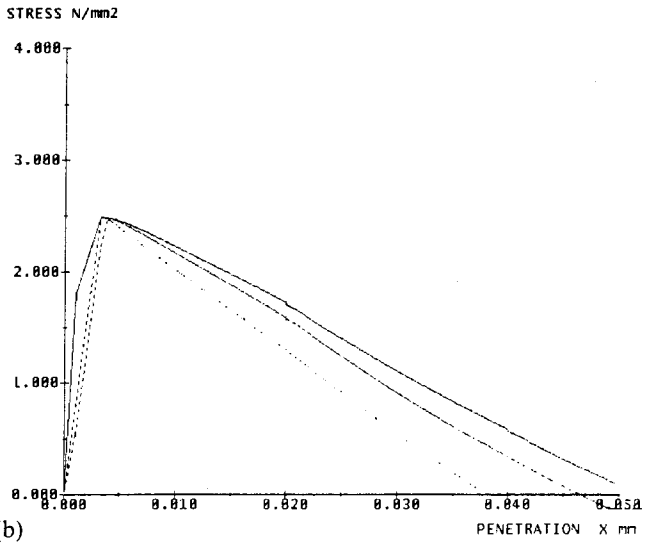


(b)

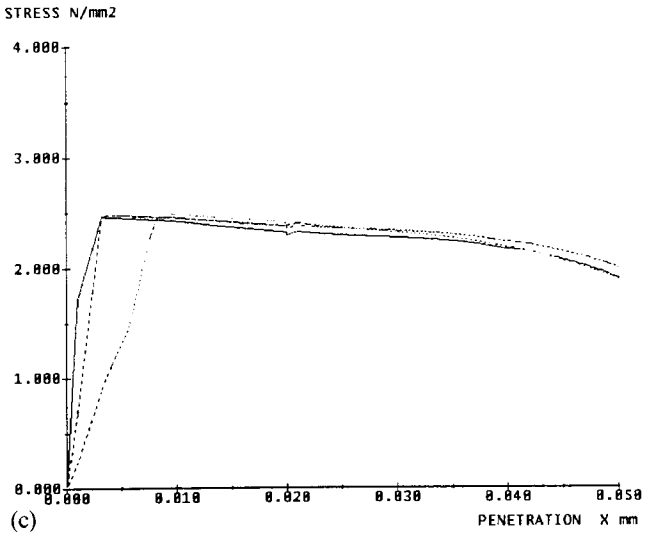


(c)

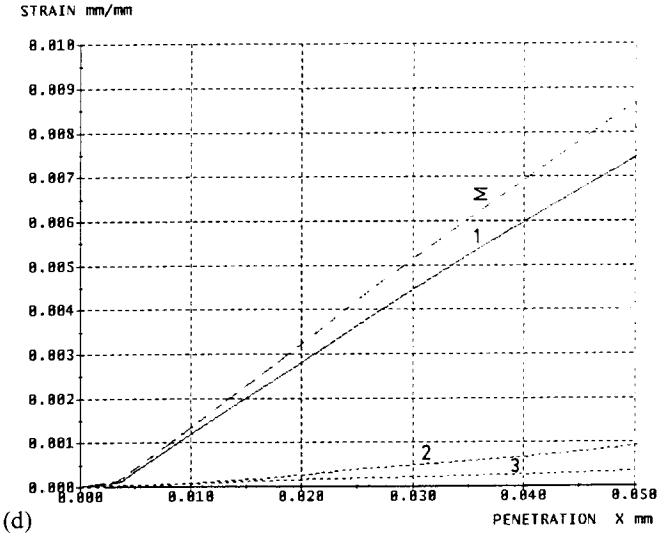


(d)

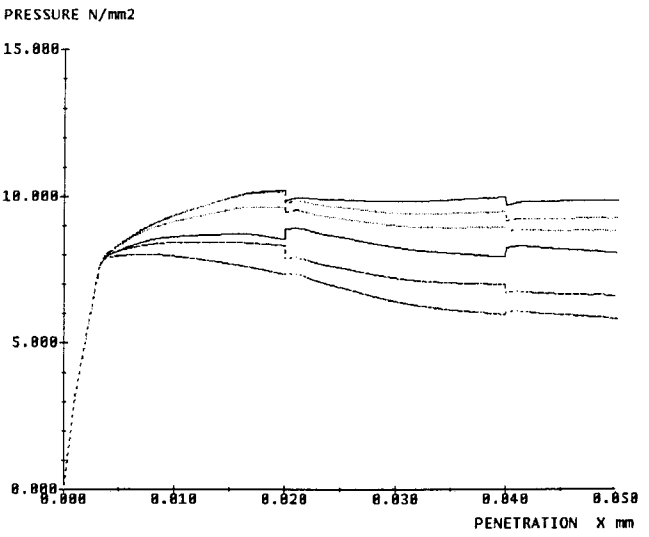


(e)

Fig. E2 Results for specimen I (tensile strength diminished): (a) deformed mesh with cracks, (b) normal stress at main crack, (c) normal stress at secondary crack, (d) average normal strain, (e) pressure at rebar.

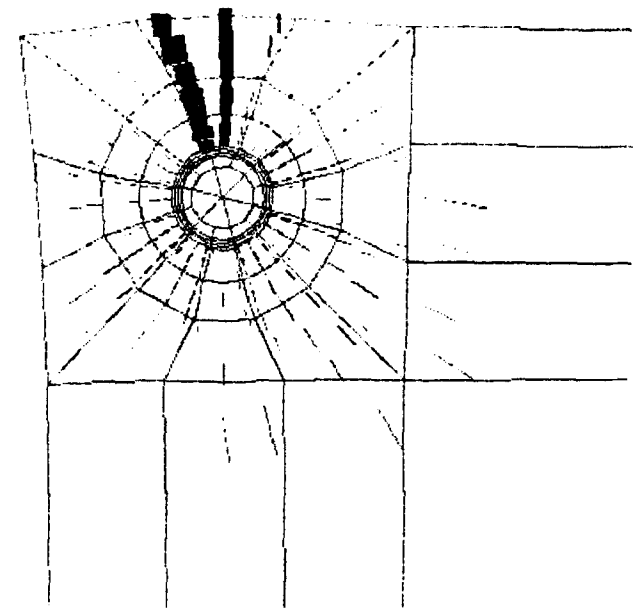

(a)

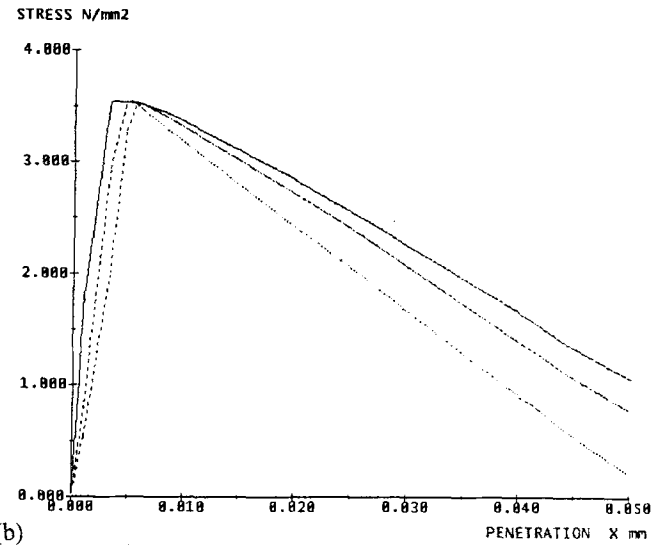


(b)

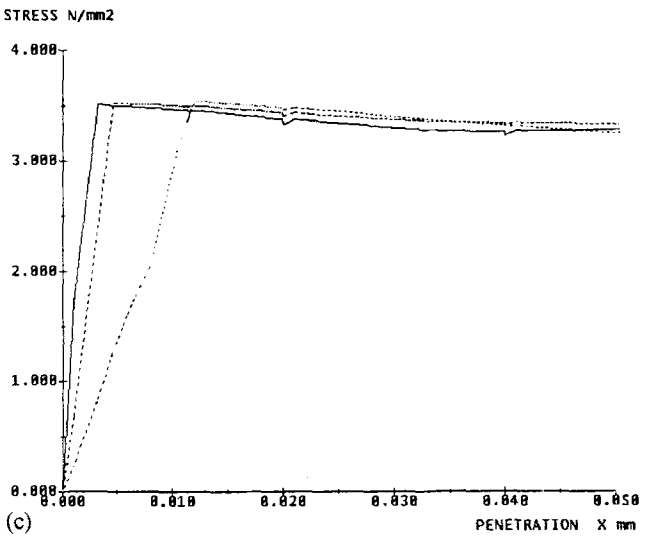


(c)

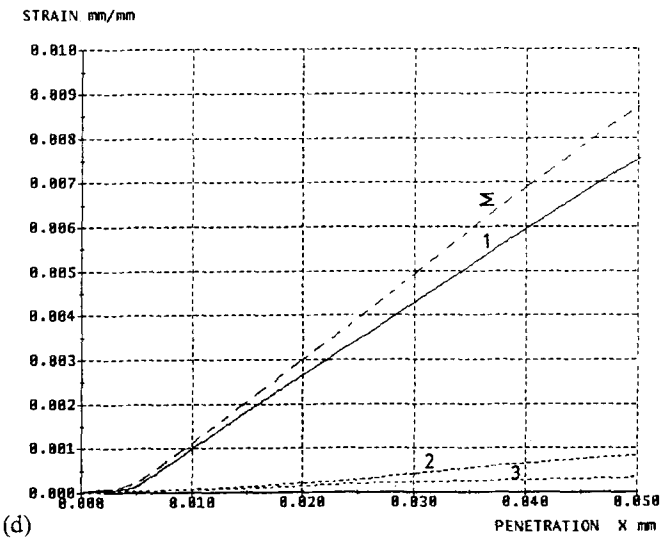


(d)

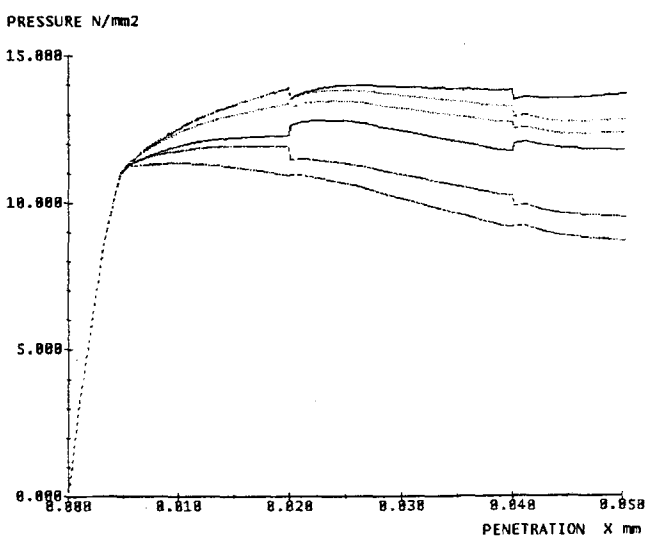


(e)

Fig. E3 Results for specimen I (fracture energy augmented): (a) deformed mesh with cracks, (b) normal stress at main crack, (c) normal stress at secondary crack, (d) average normal strain, (e) pressure at rebar.

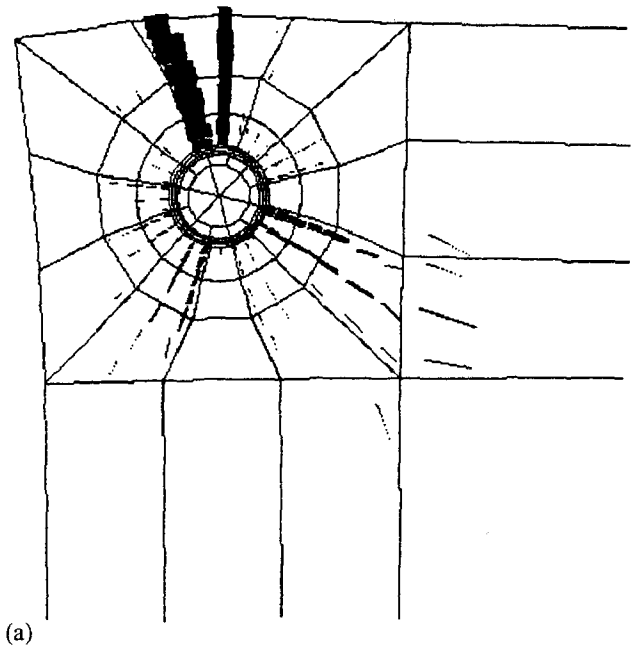

(a)

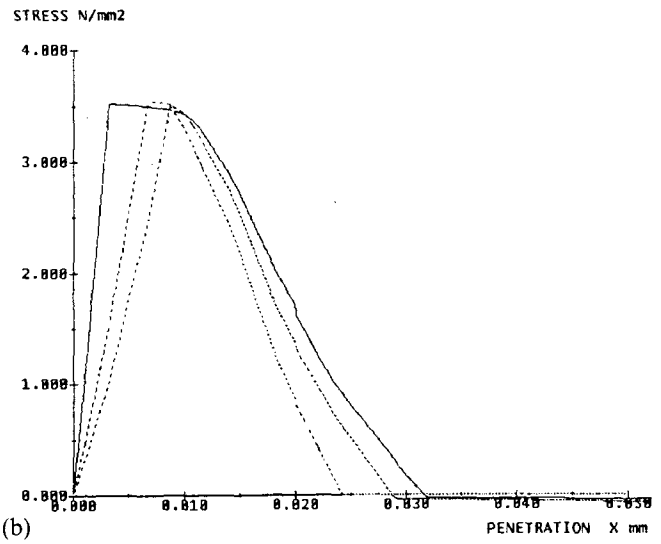


(b)

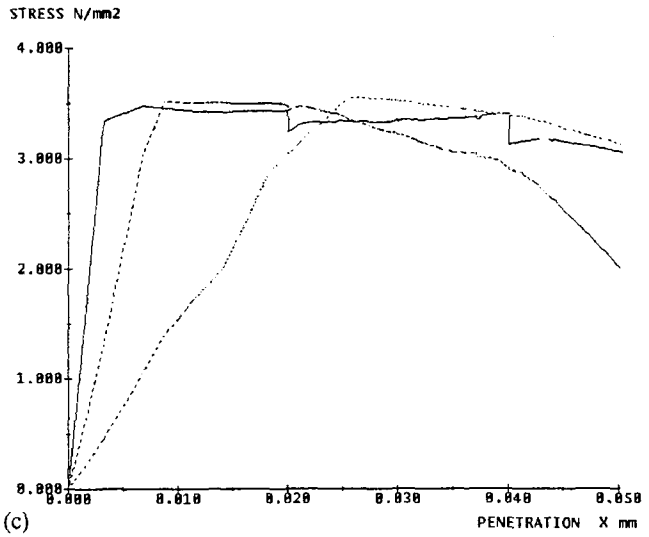


(c)

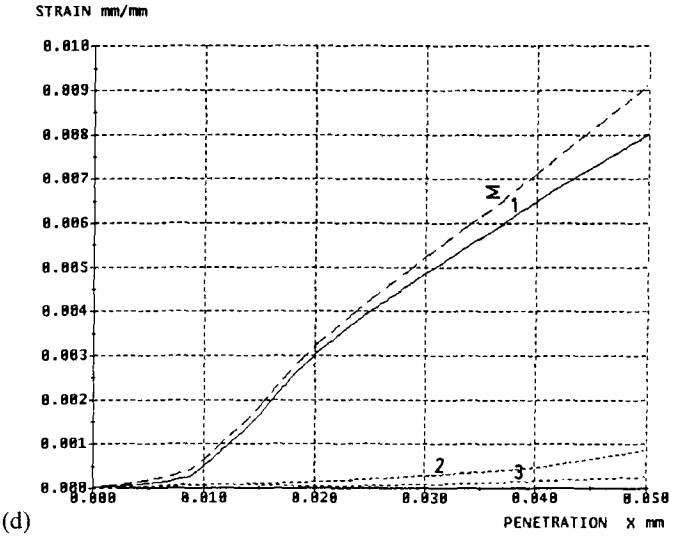


(d)

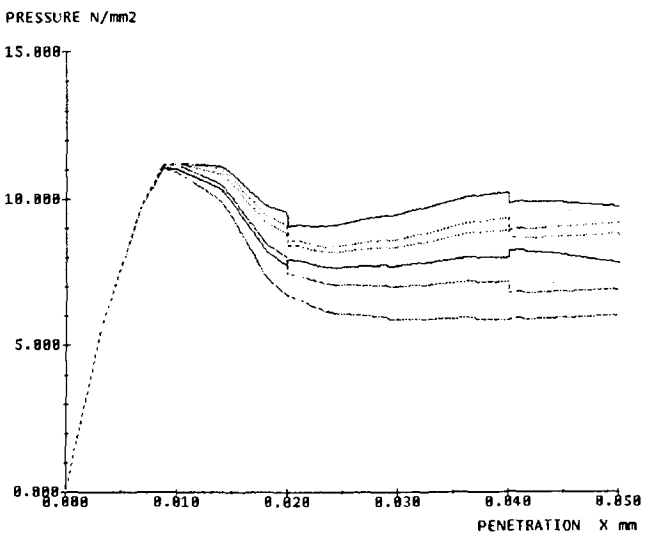


(e)

Fig. E4 Results for specimen I (Young's modulus of concrete diminished): (a) deformed mesh with cracks, (b) normal stress at main crack, (c) normal stress at secondary crack, (d) average normal strain, (e) pressure at rebar.

$v_{r/s} = 3.0$ in Fig. E1, seems to be an exact doubling of the speed in all the phenomena. In fact, that is precisely what Equation 12 would have predicted for the asymptotic global crack-width rate, since the relative increment in the specific volume has been doubled with respect to the original value.

If the tensile strength is diminished to $f_{ct} = 2.5$ MPa (Fig. E2), the peak values of the normal stresses and pressures are likewise diminished, but the cracks keep non-zero normal stress at larger widths because the fracture energy was not altered. However, the crack-width rate is only slightly affected.

Likewise, it can be seen in Fig. E3 how the effect of a greater fracture energy, i.e. $G_f = 400$ J m$^{-2}$, is very similar to the previous one, except for the fact that the peak values of the stresses and pressures are unaltered with respect to the original.

In Fig. E4 the Young's modulus of the concrete was diminished to $E_c = 20$ GPa which resulted in 'lazy' behaviour because the cracks appeared later and were also propagated later in a centrifugal sense. This effect causes a delay in the maximum stresses and pressures and in the first part of the crack growth graph, but once the cracks have been propagated, the response returns to the original line and the measurable crack widths are even a bit larger.

Finally, the value of the bulk modulus of the rust was doubled to $K_r = 4.0$ GPa which gave no significant change in the results (not included). This surprising effect is probably due to the fact that the elastic deformation absorbed by the thin layer of rust is almost negligible in the whole model.

## ACKNOWLEDGEMENTS

We are grateful to Dr J Rodríguez for his useful comments and to the Comisión Interministerial de Ciencia y Tecnología (CICYT) of the Ministry of Education and Science of Spain for having supported this research.

## REFERENCES

1. Andrade, C., Alonso, C. and Molina, F. J. 'Cover cracking as a function of bar corrosion: Part I—Experimental test', *Mater. Struct.* **26** (1993) 453–464.
2. Sygula, S. and Ryz, K. 'Longitudinal cracking and its relation to service life of reinforced concrete bridges', in Proceedings of ACI–RILEM Symposium on *Long-Term Observation of Concrete Structures*, Budapest, 1984, pp. 182–192.
3. McLeish, A., 'Cracking due to corrosion'. Technical Note No. 1632 (Taywood Engineering Research Laboratories, Southall, UK, 1986).
4. Molina, F. J. and Alarcón, E., 'Modelado numérico de la fisuración for corrosión de armaduras', *ICCET Hormigón y Acero* **175** (1990) 127–132.
5. Zienkiewicz, O. C., 'The Finite Element Method' (McGraw-Hill, London, 1977).
6. Rots, J. G., Nauta, P., Kusters, G. M. A. and Blaawendraad, J., 'Smeared crack approach and fracture localization in concrete', *Heron* **30** (1985) 1–48.
7. Rots, J. G. and Blaawendraad, J., 'Crack models for concrete: discrete or smeared. Fixed, multi-directional or rotating?', *ibid.* **34** (1989) 1–59.
8. Reinhardt, H. W., Cornelissen, H. A. W. and Hordijk, D. A., 'Tensile tests and failure analysis of concrete', *ASCE J. Struct. Engng.* **112** (1986) 2462–2477.
9. Allan, M. L. and Cherry, B. W., 'Factors controlling the amount of corrosion for cracking in reinforced concrete', in 'Corrosion 91', Proceedings of Conference and Show in Cincinnati, Ohio (NACE, Houston, Texas, 1991).
10. Hillerborg, A., Modeer, M. and Peterson, P. E., 'Analysis of crack formation and crack growth in concrete by means of fracture mechanics and finite elements', *Cem. Concr. Res.* **6** (1976) 773–782.
11. Rots, J. G., 'Computational Modelling of Concrete Fracture', Dissertation, Delft University of Technology (1988).

## RESUME

**Fissuration du béton en fonction de la corrosion de l'armature: Partie 2—Modèle numérique**

*On propose un modèle numérique basé sur des techniques normalisées d'éléments finis pour la simulation de la fracture d'échantillons de béton armé lorsque leurs armatures sont soumises à la corrosion.*

*On utilise une technique de fissuration diffuse pour modéliser le comportement des éléments finis du béton, tandis que la corrosion, qui est considérée comme la charge appliquée sur la structure, est modélisée au moyen d'une combinaison de déformations initiales et d'une modification des propriétés élastiques. Celles-ci sont respectivement équivalentes à l'expansion et au ramollissement des éléments d'acier à la surface de l'armature lorsqu'ils s'oxydent.*

*Le modèle est appliqué à quatre exemples qui ont été, en même temps, essayés de façon expérimentale (voir la première partie de cet article), et on étudie séparément l'influence des divers paramètres sur la réponse. En particulier, on évalue quantitativement l'effet du volume spécifique de la rouille qui s'est formée sur la vitesse d'ouverture des fissures.*